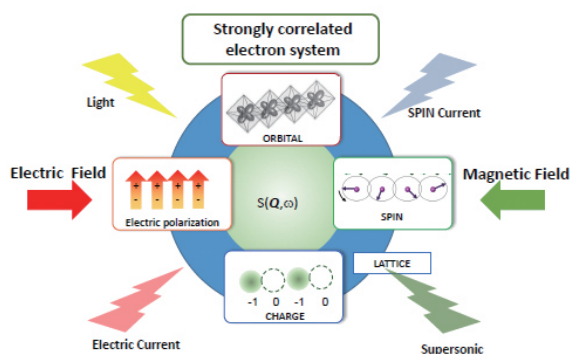


# 1 Dynamical Cross-Correlated Physics Project

## – Quantum-beam studies on dynamical cross-correlated physics in strongly-correlated-electron systems –

*Project Leader: Hajime Sagayama*

Owing to strong interelectron interactions, spin, orbital occupancy, orbital angular momentum, charge, and lattice act as degrees of freedom, and consequently, their cross-correlation dominates physical phenomena in strongly correlated electron systems. When more than one of them are simultaneously in order, such cross-correlations cause a non-conjugated external field response such as a magnetization change by applying an electric field as schematically illustrated in Fig. 1, thereby producing advanced features in a monolithic device. The objective of this project is to clarify the mechanism of the huge cross-correlation properties of strongly correlated systems from a microscopic point of view. Here, we report two studies in this project as follows:



**Fig. 1:** Schematic view of the cross-correlation among multi-degrees of freedom, spin, electric polarization, charge, orbital, and lattice in a strongly correlated electron system.

### 1-1 Electronic charge transfer driven by a spin cycloidal structure in multiferroic material

Multiferroic materials with a coupling between magnetism and ferroelectricity have been the fo-

cus of intensive research. Several studies have invited theoretical models for the mechanism of spin-driven ferroelectricity, such as “spin current (SC),” where a cycloidal magnetic structure breaks the inversion symmetry [1]. However, local ferroelectric mechanisms, such as electronic displacements driven by magnetic ordering, have remained elusive since they are expected to be small in proportion to the electric polarization in most multiferroic materials.

Recently, some resonant soft X-ray scattering (RSXS) experiments at the oxygen absorption edge for multiferroics have reported the extraction of information on electronic displacement by observing spin polarization of ligand oxygen (O) ions [2], which is induced via charge transfer from O to magnetic ions. Particularly, a recent RSXS experiment for typical multiferroic  $\text{YMn}_2\text{O}_5$  suggested that the local electronic displacement provides a major microscopic contribution to the ferroelectricity, as evidenced by a one-to-one correspondence in temperature dependence between the resonant magnetic scattering at the O  $K$  edge and the electric polarization [3]. Despite these attempts, RSXS experiments preclude quantitative discussion of the O spin polarization in evaluating the contribution of charge transfer to ferroelectricity.

Here, we focus on  $\text{YMn}_2\text{O}_5$ . This material undergoes a sequence of dielectric and magnetic phases. The magnetic structures in these phases are characterized by the magnetic wave vector  $\mathbf{q}_M$ ;  $\mathbf{q}_M = (1/2, 0, 1/4)$  for a commensurate magnetic (CM) phase and  $\mathbf{q}_M = (1/2+d_x, 0, 1/4+d_z)$  for an incommensurate magnetic (ICM) phase at low temperature. The magnetic structure in the CM phase is shown in Fig. 2 (a). The magnetic moments of  $\text{Mn}^{4+}$  form a cycloidal magnetic chain

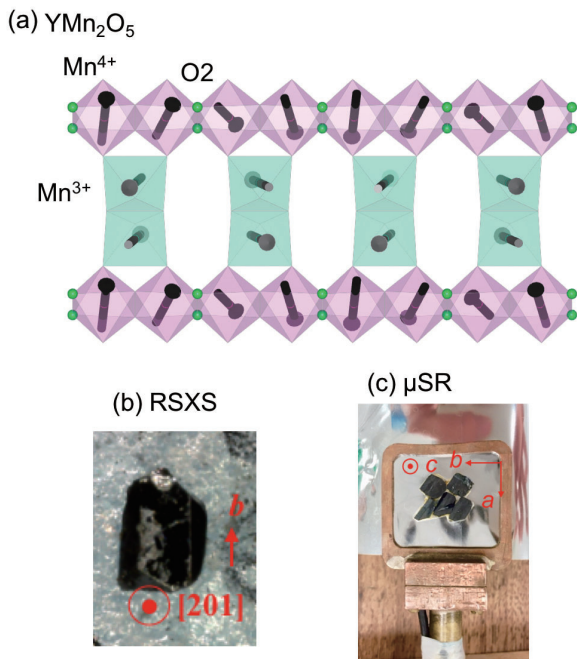


**Fig. 2:** (a) Magnetic structure of  $\text{YMn}_2\text{O}_5$ . Sample alignment for (b) RSXS and (c)  $\mu\text{SR}$  measurement.

along the  $c$ -axis, which drives the ferroelectricity in the ICM phase via the SC model. In the present study, we observed spin polarization at ligand O sites in  $\text{YMn}_2\text{O}_5$  by the synergetic use of RSXS and muon spin rotation ( $\mu\text{SR}$ ) as mutually complementary techniques.

The  $\mu\text{SR}$  experiment enables one to investigate the magnitude of O spin polarization; positive muon as pseudo-hydrogen exhibits a strong tendency to form OH bonds with oxygen ligands, thus serving as a sensitive probe for the spin polarization of O ions. We performed RSXS experiments at BL-16A at the Photon Factory, KEK, Japan, and  $\mu\text{SR}$  experiments at M15 and M20 beamlines at TRIUMF, Canada. Figure 2(b) and 2(c) show the alignment of single crystals for the RSXS and  $\mu\text{SR}$  experiments, respectively.

Figure 3(a) shows the RSXS energy spectra around the O  $K$ -edge obtained for  $\text{YMn}_2\text{O}_5$ . A well-defined peak observed around  $E = 530$  eV indicates the presence of a spin-polarized  $2p$  orbital at O sites via charge transfer from Mn to O ions. To extract information on the O spin polarization, we measured the azimuthal dependence of the resonant intensity. The data are shown in Fig. 3(b). By definition,  $\psi = 0^\circ$  indicates that the  $b^*$  axis is perpendicular to the scattering plane. The resonant intensity increases as the azimuthal angle approaches  $\psi = 90^\circ$ . The line represents

the calculated angle dependence for the magnetic structure of O ions, obtained by the present  $\mu\text{SR}$  experiment (see below).

For the  $\mu\text{SR}$  study, it is necessary to narrow down the candidate muon sites. Thus, we carried out first-principle calculations and the muon Knight shift measurements, which suggest that major muons are located near an oxygen (O<sub>2</sub>) site (see Fig. 2(a)) in all magnetic phases. The details of these results are found in Ref. [4]. Figure 4 (a) shows the time spectra at 32 K in the CM phase with the initial muon spin polarization ( $\mathbf{P}_\mu$ ) parallel to the  $c$  and  $a$  axis. In both cases, muon spin precession signals were clearly observed. The corresponding frequencies are obtained by curve fitting using the following equation:

$$A(t) = \sum A_i \cos(\omega_i t + \phi) \exp(-\lambda_i) + C$$

where  $A_i$  is the partial asymmetry,  $\omega_i$  is the muon spin precession frequency,  $\phi$  is the initial phase,  $\lambda_i$  is the transverse relaxation rate, and  $C$  is a constant component.

We first calculated the local magnetic field  $\mathbf{B}_{\text{loc}}$  at muon sites assuming that magnetic moments appear only at Mn sites in the CM phase obtained by neutron scattering experiment [5]. We found that the calculated magnitude of  $\mathbf{B}_{\text{loc}}$  is quite dif-

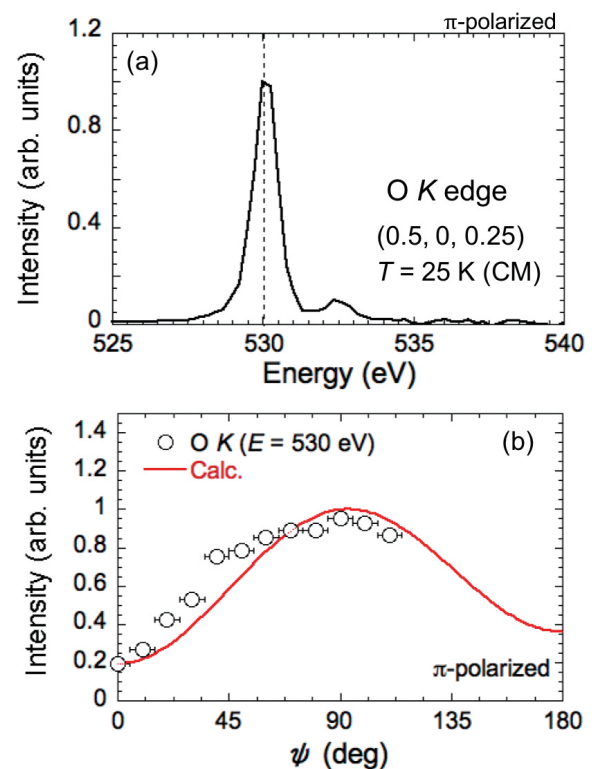


**Fig. 3:** (a) RSXS spectrum around O  $K$  edge. (b) Azimuthal dependence of resonant intensity at  $E = 530$  eV.

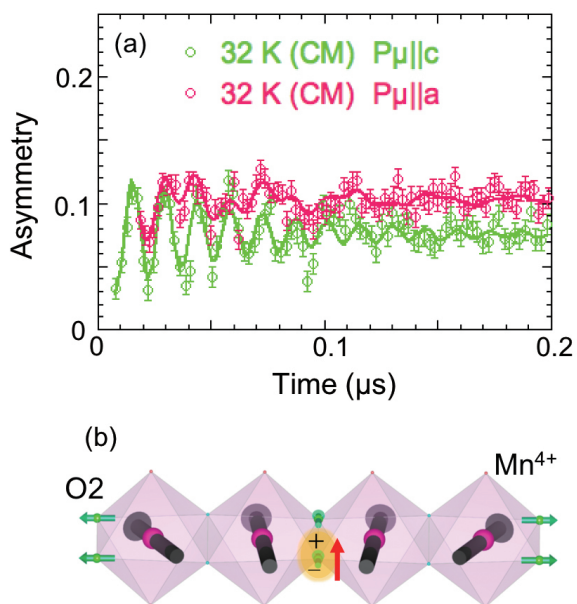


**Fig. 4:** (a)  $\mu$ SR time spectra at  $T = 32$  K with  $\mathbf{P}_\mu \parallel c$  and  $\mathbf{P}_\mu \parallel a$ . (b) Magnetic structure of O2 ions.

ferent from the experimental value. Then, we presumed the appearance of magnetic moments at the O2 site with their direction parallel to a local magnetic field exerted from the neighboring  $\text{Mn}^{4+}$  moments (see Fig. 4(b)). The calculated value of  $\mathbf{B}_{\text{loc}}$  was in excellent agreement with those deduced experimentally when the O2 moment size was assumed to be  $0.1 \mu_B$ . We also calculated the azimuthal angle dependence of the RSXS intensity at the O  $K$  edge, which is shown as a red curve in Fig. 2 (b). The reasonable agreement with experimental observations supports the appearance of spin polarization at the O2 site.

According to the  $\mu$ SR experiment at  $T = 10$  K in the ICM phase, we found that the magnitude of magnetic moments at the O2 site increased in the ICM phase. Meanwhile, recent neutron scattering experiments have demonstrated that the magnitude of vector spin chiral components increases in the ICM phase, which plays a key role in the SC model [6]. Considering that the cycloidal magnetic structure is formed via O2 ions (see Fig. 4(b)), our results strongly suggest that the SC mechanism is the primary case for the charge transfer from O2 to  $\text{Mn}^{4+}$  ions, thus leading to the local electric and spin polarization of O2 sites in  $\text{YMn}_2\text{O}_5$ .

### 1-2 Checkerboard charge density wave (CDW) and concomitant transverse-type lattice modulation formed in $\text{BiS}_2$ superconductor

Since the discovery of superconductivity in

$\text{Bi}_4\text{O}_4\text{S}_3$  [7] and  $\text{LaO}_{1-x}\text{F}_x\text{BiS}_2$  [8] in 2012,  $\text{BiS}_2$ -layered superconductors have attracted considerable attention owing to their unconventional features of superconductivity and anomalous physical phenomena [9].  $\text{RO}_{1-x}\text{F}_x\text{BiS}_2$  ( $R$ : rare-earth ion) compounds crystallize in a tetragonal structure with the space group  $P4/nmm$ , in which double  $\text{BiS}_2$  layers and  $\text{RO}$  block layers are alternately stacked along the  $c$  axis, as depicted in Fig. 5. Superconductivity arises in these materials when divalent oxygen ions are partially substituted with monovalent fluorine ions; thereby, the electron doping changes the band insulator to the metal. Increasing the ratio of fluorine substitution enhances the superconducting transition temperature ( $T_c$ ), which reaches a maximum at approximately  $x = 0.5$ . Despite extensive research, the superconducting pairing mechanism of  $\text{RO}_{1-x}\text{F}_x\text{BiS}_2$  remains a subject of debate.

First-principles calculations of  $\text{RO}_{1-x}\text{F}_x\text{BiS}_2$  indicate that the two-dimensional conduction bands consist of Bi  $6p$  and in-plane S ( $S_1$ )  $3p$  electron orbitals [10]. The Fermi surface has a rectangular parallelepiped shape that induces strong Peierls-type instability, which is expected to drive some long-range lattice modulation in  $\text{LaO}_{0.5}\text{F}_{0.5}\text{BiS}_2$  [11]. Recently, we found the superlattice structure in this material with  $\mathbf{q}_{\text{lat}} = (\zeta, \zeta, 0.5)$ , where  $\zeta \sim 0.207$  below  $T^* = 260$  K using a synchrotron radiation X-ray diffraction technique (see the reference for details [12]). Figures 6(a) and 6(b) show representative examples of X-ray oscillation photographs observed at 300 K and 30 K, respectively. None of the fundamental reflection splits, which suggests that the structure remains tetragonal even at 30 K. The existence of higher-order reflections ( $2\zeta, 0,$

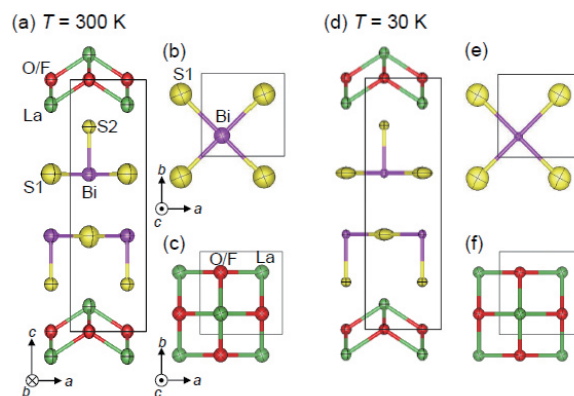


**Fig. 5:** Crystal structures of  $\text{LaO}_{0.5}\text{F}_{0.5}\text{BiS}_2$  at  $T = 300$  K and 30 K. Each ion is depicted as an anisotropic thermal ellipsoid. The black rectangles indicate the unit cell.

0) indicates not multiple domains of a single- $q$  lattice modulation but a double- $q$  lattice modulation. As shown in Figs. 7(a) and 7(b), satellite peaks of  $(0, 0, L)$  are absent in any values of  $L$ , while the satellites of  $(2, 0, L)$  are clearly observed. This result indicates that the lattice modulation is of the in-plane type. Then, we found another reflection condition for the  $(H, H, L)$  satellites. As shown in Fig. 7(c), the  $(\zeta, \zeta, \pm 0.5)$  and  $(-\zeta, -\zeta, \pm 0.5)$  reflections are absent, while the  $(\zeta, -\zeta, \pm 0.5)$  and  $(-\zeta, \zeta, \pm 0.5)$  reflections are clearly observed, indicating the transverse-type modulation schematically illustrated in Fig. 7(d). To verify the occurrence of CDW formation, we evaluated the valence state of Bi via BVS analysis [13]. The valence of Bi can be expressed as

$$\frac{a^2}{4B^2} (\cos(2\pi r(2\zeta, 2\zeta, 0)) + \cos(2\pi r(2\zeta, -2\zeta, 0))),$$

where  $a$  and  $B$  are the amplitude of the lattice

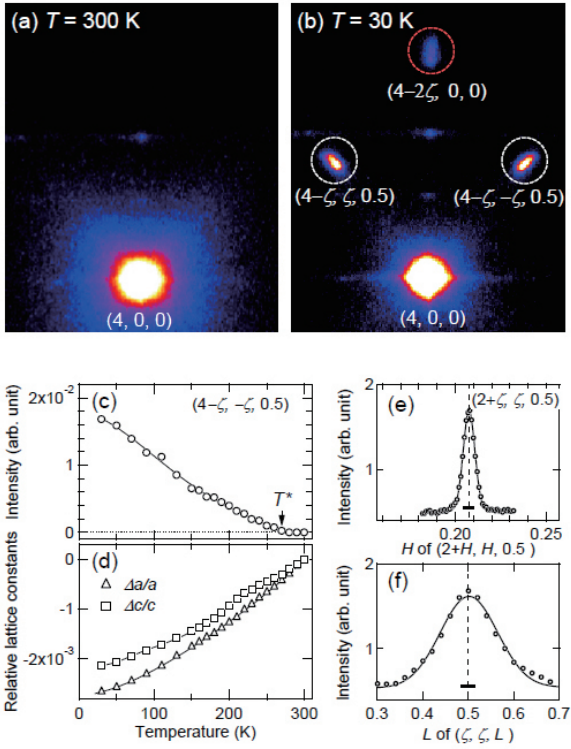


**Fig. 6:** Representative examples of X-ray oscillation photographs observed at (a) 300 K and (b) 30 K. The white and red dashed circles indicate the superlattice reflections with  $\mathbf{q} = (-\zeta, \pm\zeta, 0.5)$  and  $(-2\zeta, 0, 0)$ , respectively. (c) Temperature variation of the intensity of the  $(4-2\zeta, 0, 0)$  reflection. (d) Temperature variation of the relative lattice constants  $a$  and  $c$ . Profiles of the  $(2+\zeta, \zeta, 0.5)$  reflection scanned along (e)  $(H, H, 0)$  and (f)  $(0, 0, L)$ . The bold horizontal marks indicate the experimental resolution.

modulation and a constant value for the BVS analysis, respectively. Fig. 7(e) shows the mapping of the charge density using the equation. The Bi valence with double- $q$  modulation ( $\mathbf{q}_{\text{cdw}} = (2\zeta, 2\zeta, 0)$  and  $(2\zeta, -2\zeta, 0)$ ) exhibits a checkerboard-like CDW. It is noteworthy that  $\mathbf{q}_{\text{cdw}}$  is almost coincident with one of the predicted nesting vectors, that is,  $(0.4, 0.4, 0)$  or  $(0.4, -0.4, 0)$  [10]. This finding strongly indicates that the CDW formation should originate from the Peierls instability.

CDW states are often stabilized by modulation of the bond distances and thus couples with a longitudinal-type superlattice structure, where the wavenumber matches with the CDW. However, the CDW in  $\text{LaO}_{0.5}\text{F}_{0.5}\text{BiS}_2$  is concomitant not with such longitudinal-type lattice modulation, but rather with a transverse-type modulation with  $\mathbf{q}_{\text{cdw}}/2$ . In addition to the Peierls instability, lattice instability due to size-mismatch between the  $R(\text{OF})$  layer and  $\text{BiS}_2$  layer has been proposed by theoretical studies [11]. This is known as the in-plane chemical pressure (IPCP) effect, which contributes to the emergence of superconductivity in  $\text{BiS}_2$  materials [14]. The transverse mode around  $\mathbf{q}_{\text{lat}}$  may

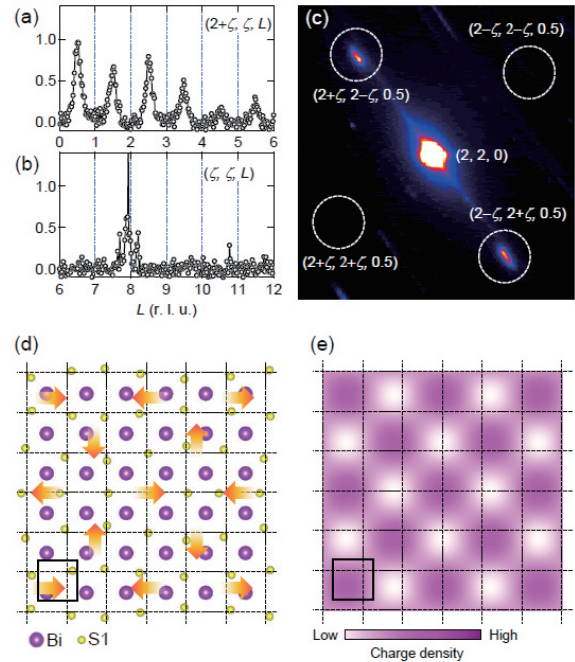


**Fig. 7:** Reflection profiles for (a)  $(2+\zeta, \zeta, L)$  and (b)  $(\zeta, \zeta, L)$  observed at 10 K. A small peak around  $(\zeta, \zeta, 8)$  is contamination from the tail of the  $(0, 0, 8)$  reflection. (c) Oscillation photograph of the  $(2, 2, 0)$  reflection and its satellites observed at 30 K. (d) Schematic illustrations of the S1 lattice modulation. The arrows demonstrate the modulation of S1 ions. (e) Schematic illustrations of the Bi valence modulation.

become more unstable than the longitudinal mode around  $q_{\text{cdw}}$  owing to the IPCP effect.

### References

- [1] H. Katsura, et al., Phys. Rev. Lett. **95**, 057205 (2005).
- [2] T. A. W. Beale, et al., Phys. Rev. Lett. **105**, 087203 (2010).
- [3] S. Partzsch, et al., Phys. Rev. Lett. **107**, 057201 (2011).
- [4] Y. Ishii, H. Sagayama, et al., Phys. Rev. B Editors' Suggestion, accepted.
- [5] Y. Noda, private communication.
- [6] S. Wakimoto, et al., Phys. Rev. B **88**, 140403(R) (2013).
- [7] Y. Mizuguchi, et al., Phys. Rev. B **86**, 220510 (2012).
- [8] Y. Mizuguchi, et al., J. Phys. Soc. Jpn. **81**, 114725 (2012).
- [9] Y. Mizuguchi, J. Phys. Soc. Jpn. **88**, 041001 (2019).
- [10] H. Usui, et al., Phys. Rev. B **86**, 220501(R) 2012; H.Usui, and K. Kuroki, Nov. Supercond. Mater. **1**, 50–63 (2015).
- [11] T. Yildirim, Phys. Rev. B **87**, 020506 (2013).
- [12] J. Kajitani, H. Sagayama et al., under submission
- [13] W. Liu and H. H. Thorp, Inorg. Chem. **32**, 4102 (1993).
- [14] Y. Mizuguchi, et al., Sci. Rep. **5**, 14968 (2015).